Modal mineralogy of carbonaceous chondrites by X-ray diffraction and Mössbauer spectroscopy

Philip A. BLAND,[1, 2*] Gordon CRESSEY,[2] and Olwyn N. MENZIES[1, 2]

[1]Department of Earth Science and Engineering, Royal School of Mines, Exhibition Road, Imperial College London
South Kensington Campus, London SW7 2AZ, UK
[2]Department of Mineralogy, Natural History Museum, Cromwell Road, London SW7 5BD, UK
[*]Corresponding author. E-mail: p.a.bland@imperial.ac.uk

Abstract–Carbonaceous chondrites are among the most analyzed geological materials on Earth. However, despite this attention, and unlike most terrestrial rocks, little is known on the abundance of individual phases within them. Here, we show how a combination of several novel X-ray diffraction (XRD) techniques (including a high-brightness X-ray MicroSource®), and Mössbauer spectroscopy, allows a complete modal mineralogy to be ascertained from even the most highly unequilibrated, fine-grained chondrites for all minerals of abundance >1 wt%. Knowledge of the modal mineralogy of a sample also allows us to calculate grain density.

We analyzed Allende, Murchison, Tagish Lake, and Orgueil. Based on our modal data, the grain density estimates for Allende, Murchison, and Orgueil are close to literature values. In the case of Tagish Lake, there is no published grain density, although a bulk density measurement does exist. Taking our estimate of grain density, and the measured bulk density, we calculate an exceptionally high porosity of 41% for this meteorite, similar to some chondritic IDPs and in line with a porosity calculated from an entry model for the Tagish Lake fireball. Although it is an oxidized CV, magnetite is present in Allende at a level of <0.5 wt% or <0.3 vol%, a result that is substantiated by several other instrumental studies. This may be an oxidized meteorite, but that oxidation is not manifested in abundant magnetite. In addition, we note appreciable fayalitic olivine in Orgueil, detected by both XRD and Mössbauer. We employed MicroSource® XRD to look at heterogeneity in mineral abundance in Orgueil and found substantial variation, with phyllosilicates varying inversely with olivine. The data suggest that Orgueil was initially composed primarily of anhydrous materials, which have been partially, but not completely, altered.

Although the data are preliminary, comparison between our XRD modal assessment, bulk chemistry, grain density, and Mössbauer data, suggests that our estimates of mineral abundance are robust. The advent of MicroSource® XRD allows similar modal data to be acquired from samples as small as a few hundred micrograms.

INTRODUCTION

Comparatively few estimates exist for the abundance of individual phases in chondritic meteorites. Normative abundances, recalculated from chemical analyses, have been attempted (e.g., for equilibrated ordinary chondrites [McSween et al. 1991]), but in heterogeneous unequilibrated chondrites, such studies are hampered by a lack of information on the average composition of individual phases and on the presence of hydrous minerals. Point counting is similarly limited by the fine-grained nature of most unequilibrated chondrites. More recently, instrumental methods have been applied to this problem (Bland et al. 1997, 1999, 2000a, b, 2002; Bland and Cressey 2001; Menzies et al. 2001, 2002). Mössbauer spectroscopy detects Fe-bearing phases, even if crystallinity is poor and grain size is small (<50 nm). XRD detects all crystalline phases above ~50 nm in size. In this paper, we employ a number of novel XRD techniques not only to identify phases but, also, to quantify their abundance and quantify the range of olivine compositions within an unequilibrated chondrite. Mössbauer spectroscopy is used to help define the Fe-containing mineralogy in a sample and, in some cases, to confirm XRD modal assessments. Knowledge of the complete modal mineralogy of a sample also allows us

to calculate the grain density of each meteorite. Aside from providing an independent check on our abundance estimates, this method is also an attractive non-invasive alternative to grain density determination using helium pycnometry. Since bulk density may now be determined in a non-invasive manner (Consolmagno and Britt 1998), density and porosity determinations can be made on meteorites with a minimum of contamination.

SAMPLES AND METHODOLOGY

Samples of bulk Allende, Murchison, Tagish Lake, and Orgueil (0.2–0.3 g) were prepared for XRD and Mössbauer spectroscopy by grinding. In the case of meteorites that contain large (cm-scale) inclusions, such as Allende, care was taken to avoid these in selecting samples for analysis. Although in earlier work we crushed samples under acetone to prevent oxidation (e.g., Bland et al. 1995), the effect was found to be minimal and undetectable by Mössbauer spectroscopy. Subsequently, samples were crushed in air. Aside from crushing, XRD and Mössbauer analysis is non-destructive, so ground samples are available for additional analysis. Grain size variability is an issue in XRD analyses, so care was taken during grinding that a uniform fine (<35 micron) grain size was achieved to allow a smooth powder surface for the XRD experiments. Reproducing the powder surface topography of each sample in this way ensures that microabsorption (beam attenuation due to surface roughness) is minimized, as demonstrated by Cressey and Batchelder (1998). In most cases, large samples were obtained to increase the probability of deriving a modal mineralogy that is relevant to the whole meteorite. These were analyzed by XRD using a well with a volume of 180 mm³. To investigate sample heterogeneity, we used a high-brightness X-ray source that allows analysis of much smaller samples. A custom designed micro-well of a volume of 0.07 mm³ was used to analyze aliquots of Orgueil of a few hundred μg in mass, from which modal mineralogy data could be derived and compared to the larger bulk.

In addition to the meteorites, a large number of mono-mineralic standards were analyzed to aid XRD modal assessment. These included a wide range of synthetic olivine standards of compositions spanning the solid solution series.

X-RAY DIFFRACTION METHODOLOGY

Modal Mineralogy by XRD

XRD data were collected using an INEL curved position-sensitive detector (PSD) with an output consisting of 4096 channels (each 0.03° 2θ wide) representing a total arc of about 120° 2θ, enabling diffraction patterns to be collected simultaneously at all angles. In curved PSDs, an intense electric field is applied close to a curved anode, designed as a very thin curved blade. Each X-ray photon hitting the detector ionizes the counting gas, causing a fast multiplication phenomenon, or so-called "avalanche." On the cathode readout, an inducted charge arrives perpendicular to the impact point of the avalanche. The position of this charge is determined by the delay-line method. This charge is carried away by 2 pulses travelling to either end of the delay line and arriving there at different times. Measuring the time difference between the 2 pulses effectively localizes the incident photon in the detector.

Cressey and Schofield (1996) first described the method for rapid and effective phase quantification of multiphase samples using PSD instrumentation, and we have used a similar experimental configuration in this study. Cu$K\alpha_1$ radiation was selected using a Ge111 monochromator, and post-monochromator slits were used to restrict the beam to 0.24×5.00 mm, with the long dimension of the beam parallel to the axis of the PSD curvature. For the large samples, each powder sample was packed into a circular plastic well 15 mm in diameter and 1 mm deep. Silicon was used as an external standard for the 2θ calibration of the detector. The 2θ linearization was performed with GUFI software using a least-squares cubic spline function. Diffraction patterns were recorded in reflection geometry, from the flat top surface of the sample powder, set at 13° to the incident beam, with the sample surface slowly spinning in its own plane; this is the only movement in the XRD-PSD system and does not alter the static beam-sample-detector geometry. The reproducibility of this static experimental geometry from one sample to the next is extremely high because nothing moves. This is unlike a conventional Bragg-Brentano scanning diffractometer where the θ–2θ coupled movement can easily become imprecise. The need for mechanical movement of such systems together with the commonly encountered differences in the degrees of preferred orientation present in each sample can easily upset the precision and accuracy in phase quantification attempts. Many different methods have been suggested for producing randomly oriented crystallite sample mounts for use in conventional scanning diffractometry, but these are difficult, time consuming, and often unsuccessful. The XRD-PSD static geometry, together with the simple powder sample preparation we employ of top-loading the well holder to produce a smooth surface tamped down with the narrow-edge (not the flat side) of a spatula, results in a near-random set of Bragg orientations being detected by the PSD over 120° 2θ. This does not necessarily mean that the sample mounts we prepare have perfectly random crystallite orientations, although the degree of randomness is certainly high. More importantly for phase proportion analysis, we can attain reproducible whole-pattern intensities with ease between consecutive mounts, even when prepared by different operators. The combination of static experimental geometry and the sample preparation method we employ is the main reason for the much-improved phase quantification results possible with the XRD-PSD method

compared to those normally obtained by conventional (scanning diffractometer) systems. Also, unlike many other methods using XRD for phase quantification, the XRD-PSD method does not require spiking with an internal standard powder and, thus, completely avoids contaminating the sample material.

The XRD-PSD method for rapid phase quantification was first introduced by Cressey and Schofield (1996) and was further developed by Batchelder and Cressey (1998), who incorporated new procedures to correct for differences in attenuation of the diffracted radiation by the multiphase sample and by the single-phase standards. Both these studies demonstrate that accurate and reproducible phase quantification is possible for a diverse range of complex mixtures. The XRD-PSD phase quantification procedure using whole-pattern fitting can be summarized by the expression:

$$X_i = \left(\frac{t'}{t}\right)\left(\frac{I'_0}{I_0}\right)\left[\frac{(\mu/\rho)_i}{(\mu/\rho)'}\right]w_i \tag{1}$$

where X_i is the pattern intensity fraction from phase i in the mixture relative to the intensity of a standard pattern of pure i (intensity = 1.0), t and t' are the counting times for the standard and mixed assemblage patterns, respectively, I_0 and I_0' represent the incident beam flux during acquisition of standard and mixed assemblage patterns, respectively, $(\mu/\rho)_i$ is the mass absorption coefficient for phase i, $(\mu/\rho)'$ is the mass absorption coefficient for the mixture, and w_i is the actual weight fraction of phase i present in the mixture.

This relationship can be used quantitatively with any particular static geometry of the PSD system. Furthermore, standard patterns need not necessarily be acquired over a counting time period equivalent to that of any multiphase sample, as standard patterns can be proportioned by t'/t during the data analysis. Similarly, any differences in incident beam flux can be taken into account using the method described in Cressey and Schofield (1996), where the backgrounds of the external silicon calibrant patterns recorded during each experimental session are used as a relative measure of total X-ray flux at the sample. This flux correction capability has the advantage that, if necessary, standard patterns acquired many months or years earlier can be employed for preliminary phase quantification during the search for best-match standards from the database.

In the initial stage of the quantitative phase analysis, the phases present in the mixture (e.g., meteorite samples) are identified by direct comparison of the total mixture pattern with sets of actual diffraction patterns from single-phase standards from our database (sourced from The Natural History Museum collections), which are chosen to match as closely as possible the whole-pattern signatures of those materials in the mixture. For example, a best match is inherently made with each phase in terms of: degree of crystallinity, order-disorder characteristics, and solid solution composition. For each phase identified, the standard (100%

single-phase) pattern is reduced in intensity to achieve a best fit to that phase component in the multiphase (meteorite) pattern and is then subtracted to leave a residual pattern. This process is repeated until a zero residual pattern shows that all the phases in the mixture have been accounted for.

The determined pattern fit proportions are not the actual phase proportions in the mixture, and it is first necessary to make corrections for X-ray absorption in the sample relative to the standard (see Equation 1) to make this conversion. If the phase proportions were known already, the mass absorption coefficient for the mixture could be simply computed as a weighted average of the mass absorption coefficients of the constituent phases (calculated from the mass absorption coefficients for the constituent elements and the appropriate radiation given in the International Tables for X-ray Crystallography):

$$(\mu/\rho)' = \sum_i w_i(\mu/\rho)_i \tag{2}$$

But, for a mixture of unknown phase proportions or unknown bulk chemistry, calculating this actual mass absorption coefficient for the mixture is not possible. However, as pointed out by Batchelder and Cressey (1998), the true matrix absorption coefficient $(\mu/\rho)'$ is related to an apparent matrix coefficient $(\mu/\rho)''$ by a scaling factor of value (s), where $(\mu/\rho)''$ can be defined using the pattern-fit values (apparent phase proportions in the diffraction pattern):

$$(\mu/\rho)' = s(\mu/\rho)'' \tag{3}$$

$$(\mu/\rho)' = s\left[\sum_i X_i(\mu/\rho)_i\right] \tag{4}$$

The value $s(\mu/\rho)''$ may now be substituted in Equation 1, and by calculating the phase proportions as a normalized ratio, the scale factor (value s) cancels out. Thus, the actual weight fractions of each phase can be determined simply from their measured pattern-fit fractions and their calculated mass absorption coefficients:

$$w_i = \frac{X_i[(\mu/\rho)''/(\mu/\rho)_i]}{\sum_i X_i[(\mu/\rho)''/(\mu/\rho)_i]} \tag{5}$$

Therefore, the XRD-PSD system, using a curved 120° 2θ static detector, allows whole diffraction patterns of standards and multiphase mixtures to be compared directly in a simple manner and, consequently, yields accurate assessments of phase proportions by the application of a straightforward correction for absorption. Not only is this a major advance in the application of XRD to phase quantification, but this approach also allows a very rapid assessment to be made without loss of accuracy. This method has been thoroughly tested, is universally applicable to complex crystalline

mixtures, and is far easier to employ with speed and accuracy than other methods of phase quantification using XRD that have thus far been devised. An inter-laboratory round robin to test quantitative phase analysis from diffraction data was recently commissioned by the International Union of Crystallography (Madsen 1999: Madsen et al. 2001). Eight samples of a 3-phase mixture were dispatched to 128 laboratories. Eighty laboratories returned data. Only after submission of all results were the actual wt% values of the mixtures published. These are shown with our XRD-PSD results in the upper part of Fig. 1. The lower diagram shows the data spread from all participating laboratories, using conventional phase quantification methods (including Rietveld whole-pattern analysis, iterative least squares [ILS], reference intensity ratio [RIR], and internal standard techniques). Ours was the only XRD-PSD whole-pattern matching technique employed, and all our results were finalized within a few days of receipt of the samples. Clearly, the XRD-PSD offers a new, effective, and rapid means of establishing phase abundances in mixed phase samples with an accuracy of ~1% for an individual phase, provided that well-matched standard materials are available.

Cu Radiation and Fe-Containing Materials

Another interesting and novel aspect of our PSD experiments is our (deliberate) use of Cu radiation, even when investigating Fe-rich materials. This can have certain advantages in phase analysis, as outlined below.

$CuK\alpha_1$ radiation gives rise to significant background fluorescence from samples containing abundant Fe. The X-ray scattering detected by the PSD from a crystalline Fe-bearing material is composed of 2 parts: the Bragg scattering of $CuK\alpha_1$ radiation and a background fluorescence emission ($FeK\alpha$ radiation) produced by absorption of the incident $CuK\alpha_1$ radiation. The PSD pattern recorded is an additive function of these 2 different components: the peaks from crystalline phases are seen superimposed on a background fluorescence consisting of broad undulations. The exact profile of these undulations varies for each PSD but is very stable for any particular detector as it is related to the electrical resistances of the inbuilt delay lines of an individual detector. Because the background fluorescence is characteristic and reproducible for all Fe-phase patterns, this fluorescence signal can be made use of in a number of ways. Each Fe-bearing phase contributes to the fluorescence background, so we can use the relative background intensity from each phase as a relative measure of its Fe content. For example, Fig. 2 shows the variation in total pattern profiles of a series of different olivine compositions, $(Mg_xFe_{1-x})_2SiO_4$. This experiment indicates that the total intensity of the fluorescence emission is directly proportional to the abundance of Fe in the sample and inversely proportional to the X-ray absorption characteristics of the sample. Similarly, the background fluorescence intensity from a
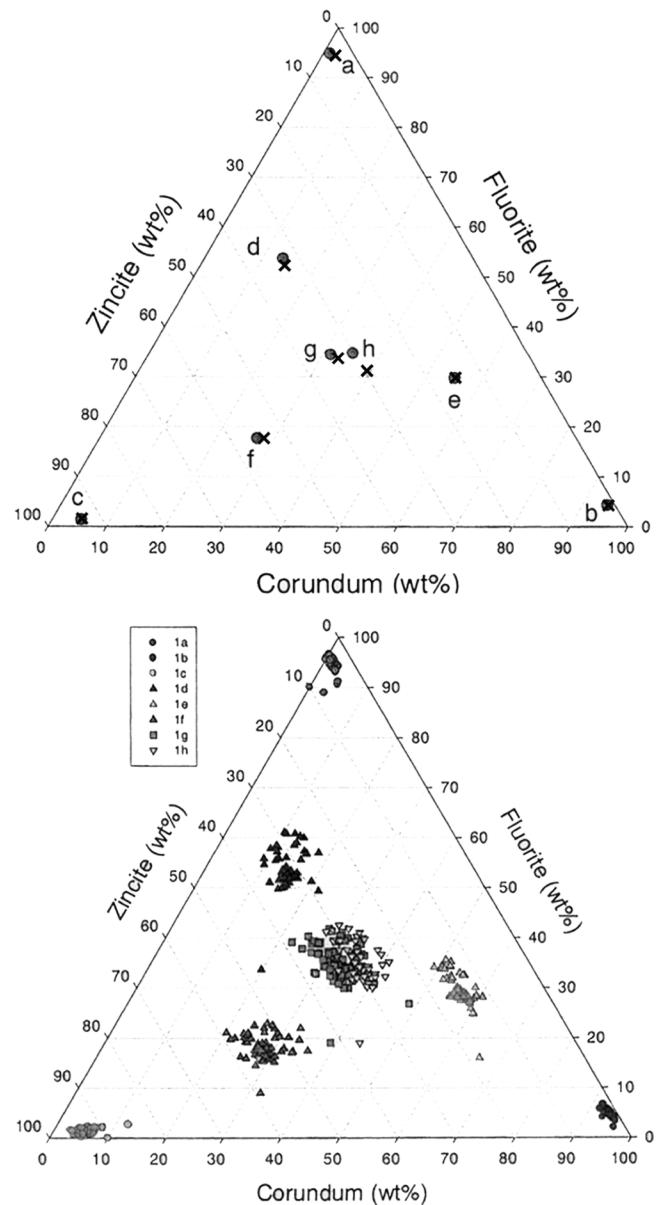
Fig. 1. Inter-lab comparison showing (in the upper ternary diagram) the close correspondence between known wt% mixtures of 3 phases prepared by the International Union of Crystallography (filled circles) and our X-ray diffraction with 120° position sensitive detector (XRD-PSD) results (crosses) and (in the lower diagram) the data returned from 80 labs in the study.

sulphide, phyllosilicate, or oxyhydroxide is distinct, as it is associated with the Fe abundance in each mineral.

Another benefit of using Cu radiation to induce strong fluorescence is that it can be used to quantify the amount of an X-ray amorphous Fe-bearing phase after first subtracting the whole-pattern profiles of any crystalline Fe-phases. In the absence of fluorescence, the weak and diffuse scattering from an amorphous phase can often go unnoticed in the total pattern and is, hence, more difficult to quantify. However,
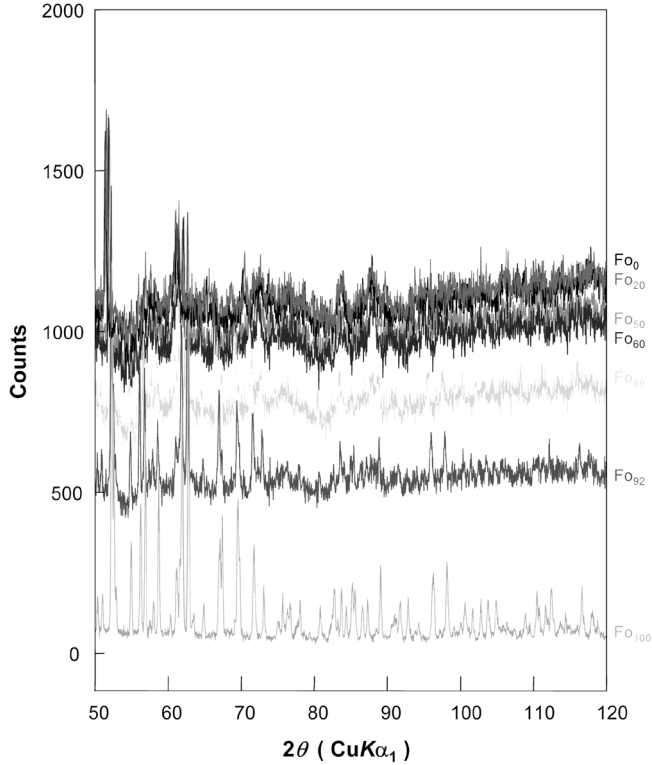
Fig. 2. XRD-PSD patterns comparing background fluorescence intensities in olivines with varying Mg-number. Samples were prepared as powders in deep-well mounts, with a 13° incidence between beam and sample and with a count time of 10 min.

fluorescence can help considerably, especially when the amorphous phase is small in amount, because the fluorescence emission is measurable even for low Fe-contents. In this respect, acquiring additional information on the full range of Fe-bearing phases present is a distinct advantage when comparing these results with our Mössbauer analyses. When assessing the proportions of amorphous Fe-phases by XRD-PSD, an additional correction must first be made to the background fit value to allow for the attenuation of the Fe$K\alpha$ radiation on its passage out of the multiphase sample relative to the 100% phase standard. For samples containing an amorphous Fe-phase, the mass absorption coefficient of the matrix for Fe$K\alpha$ radiation is given by expressions analogous to Equations 3 and 4 for Cu$K\alpha$ radiation:

$$(\mu/\rho)'^{Fe} = s^{Fe}(\mu/\rho)''^{Fe} \tag{6}$$

$$(\mu/\rho)'^{Fe} = s^{Fe}\left[\sum_i X_i(\mu/\rho)_i^{Fe} + X_{amFe}(\mu/\rho)_{amFe}^{Fe}\right] \tag{7}$$

where X_i is the pattern fit fraction for crystalline phase (i), and X_{amFe} is the pattern (background) fit fraction for the amorphous Fe-phase relative to their respective pure phase standard pattern intensities. Formulation of an analogous expression to Equation 5, but for Fe$K\alpha$ radiation, gives:

$$X_{amFe}^* = \frac{X_{amFe}\left[\dfrac{(\mu/\rho)''^{Fe}}{(\mu/\rho)_{amFe}^{Fe}}\right]}{\sum_i X_i\left[\dfrac{(\mu/\rho)''^{Fe}}{(\mu/\rho)_i^{Fe}}\right] + X_{amFe}\left[\dfrac{(\mu/\rho)''^{Fe}}{(\mu/\rho)_{amFe}^{Fe}}\right]} \tag{8}$$

where X^*_{amFe} is the fit fraction of the X-ray amorphous Fe-bearing phase after correction for attenuation of Fe$K\alpha$ fluorescence radiation. This adjustment to the fit value for the amorphous fluorescing phase will be to a higher value if the attenuation of Fe radiation by the mixture is greater than in the pure standard and to a lower value if the converse is true. The adjusted value (X^*_{amFe}) is then incorporated into Equation 5 and becomes one of the X_i component phases. Thus, the Fe-bearing amorphous phase is finally treated as though its fit fraction had been determined from long-range-order (crystalline) Bragg scattering and is incorporated into the final absorption correction along with the crystalline phases using Equation 5.

During this study, it became apparent that the modal amounts of Fe-sulphides we determined were somewhat in error. Clearly, the mass absorption coefficients of Fe-sulphides calculated for Cu$K\alpha_1$ radiation from a weighted average of the elements they contain significantly over-estimate the absorption. Apparently, the mass absorption values for metallic Fe can be transferred successfully to model the absorption characteristics of Fe in oxides and silicates. However, because the hybrid-type electronic bonding of Fe in sulphides is so different from the electronic structure around Fe atoms in oxides and silicates, the mass absorption coefficients for Fe-sulphides cannot be calculated accurately from the elemental mass absorption tables. Therefore, we have measured experimentally the mass absorption coefficients for various Fe-sulphides. Normally, such measurements are not trivial (consequently, very few mass absorption measurements for compounds exist in the literature), but using our Equation 5, this task becomes a straightforward experiment for a binary Fe-sulphide + silicon mixture in a known weighed-out proportion. Thus, Equation 5 is solved for the single unknown value $(\mu/\rho)_{Fe-sulphide}$ for Cu radiation. In this way, we have derived experimentally measured mass absorption coefficients for pentlandite, pyrrhotite, and troilite. Not surprisingly, these are very different from the values calculated from the International Tables for X-ray Crystallography (1974).

Some of the meteorite samples in this study contain X-ray-amorphous Fe-sulphides, so we also need to know the mass absorption coefficients for Fe$K\alpha$ radiation to apply Equation 8. These attenuation coefficients for Fe radiation have been calculated from the background intensity level of emitted fluorescence using the relationship found to hold for the Fe-Mg olivine series shown in Fig. 2. For a phase (i) that absorbs Cu radiation, the intensity of emitted fluorescence radiation (I_i^{fluo}) is directly proportional to its Fe content (c_{Fe})

and is inversely proportional to its mass absorption coefficients for Cu and for Fe radiation:

$$I_i^{fluo} = k \cdot c_{Fe} \cdot \frac{1}{(\mu/\rho)_i^{Cu}} \cdot \frac{1}{(\mu/\rho)_i^{Fe}} \qquad (9)$$

where the experimental constant, k, is defined as:

$$k = \frac{I_{std}^{fluo} \cdot (\mu/\rho)_{std}^{Cu} \cdot (\mu/\rho)_{std}^{Fe}}{c_{Fe}^{std}} \qquad (10)$$

k is determined by measuring the fluorescence intensity level of a standard (I_{std}^{fluo}) under the same conditions as phase (i), and expressing the result as a ratio ($I_i^{fluo}/I_{std}^{fluo}$). Equation 9 can then be solved for the single unknown parameter $(\mu/\rho)_i^{Fe}$.

Modal Mineralogy of Small Volumes of Material

The system we have described above makes use of a position sensitive detector in a novel way. We have recently developed a parallel system that also uses a PSD but employs a high-brightness X-ray generator developed by Bede Scientific Ltd. This MicroSource® generates a small cross-section X-ray beam with a brightness (flux per unit area) at least 2 orders of magnitude greater than that from a conventional sealed-tube source. In addition, the MicroSource® delivers a beam that is focused and highly collimated with a divergence angle of only 2 milliradians (0.15°). The beam is focused by specular reflectance along a capillary with an internal mirror coating, ensuring that almost all the X-rays generated, rather than being lost, are concentrated into a fine (almost parallel) beam. Beam divergence of the MicroSource® approaches that of some synchrotron sources. The system was tested initially, acquiring data from inclusions in primitive meteorites in thin section (Bland et al. 2000b). It is now optimized for analyses of extraterrestrial materials and, in addition to offering in situ investigation of mineralogy in inclusions in polished sections, also allows analysis of small (0.02–0.07 mm^3) ground samples in a micro-well, which enables full characterization of mineral abundance in small separated materials.

The micro-well must be filled with the same volume of finely powdered material each time. This was achieved, under a petrologic microscope, by an iterative process of overfilling the well and then pressing down on top with a glass slide. Any excess powder around the edge of the well was removed so that, with a second pressing with the glass slide, the powder filled out to the edge of the well. In addition to sample volume replication, it is important for mineral quantification to avoid preferred orientation effects. The use of a glass slide to flatten the sample surface may impart a preferred orientation effect, which is not possible to avoid. Preferred orientation of some reflections may occur, but the phase quantification method uses the whole pattern profile, minimizing any effect that might occur from a single peak with enhanced intensity.

A graphite monochromator was used to filter out Cu$K\beta$ wavelengths from the microbeam, which consists of a mixture of Cu$K\alpha_1$ and Cu$K\alpha_2$ wavelengths. To maintain the high intensity of the incident beam, the $K\alpha_2$ wavelengths were not filtered from the primary beam. A slit or pinhole of required dimension (pinholes as small as 50 μm can be used for these analyses) was placed in front of the X-ray beam and positioned until the portion of the beam sampled was the lower part of the bright core containing mostly $K\alpha_1$ but also some $K\alpha_2$ wavelengths. Any remnant $K\alpha_2$ wavelengths were stripped out of the pattern using conventional software.

The sample holder containing the micro-well was placed on a goniometer, which allows for manual xyz movement, to position the micro-well, at an angle of approximately 6° from horizontal, in the center of the X-ray beam. The goniometer spins around the z axis. The x and y adjustments were used to ensure both that the beam was in the center of the well and that the center of the well was in the center of rotation of the goniometer head. This was done by placing a fluorescent disk with a centrally marked black dot on the goniometer. A telescope with a focal length of ~10 cm was used to find, in focus, the position where the beam hit the fluorescent disk. The central dot was then moved, using the xy shift on the goniometer, so that it was the central point of rotation of the entire disk, i.e., of the goniometer stage. The central dot was then further adjusted by moving the entire goniometer and adjusting the z height on the goniometer so that the dot lay on the crosshairs of the telescope, i.e., the position of the beam. The beam was, therefore, aimed at a precise area that lay in focus at the crosshairs. When this position setting was achieved, neither the telescope nor the goniometer was moved for the duration of the analysis so that all of the samples and standards were run under the same conditions, and the volume analyzed by the X-ray beam was replicated each time.

Appropriate standards were run, and the data were processed in a similar manner to the larger samples using the conventional source.

[57]Fe Mössbauer Methodology

Mössbauer spectra were recorded from bulk meteorite samples at 298 K with a microprocessor-controlled spectrometer using a [57]Co/Rh source. Drive velocity was calibrated using a metallic Fe foil. Although Mössbauer spectroscopy only detects Fe-containing phases, it has the advantage of detecting any Fe nuclei bound in a lattice. In most cases, the intensity of an absorption in a Mössbauer spectrum is related to the proportion of the total iron at that site in a lattice (and often the proportion of the total iron in an individual phase). This may not always be true. Significant variability in Fe-isotope ratio between different phases in a sample, variations in the recoil-free fraction, and thickness effects can obscure a simple relationship between Fe-content and intensity. The measured Fe-isotopic variation in

meteorites does not appear to be enough to affect our estimates (Zhu et al. 2001; Mullane et al. 2003). Future work will attempt to constrain the significance of thickness effects, but here, we simply use a cross-comparison with the XRD results to check the accuracy of the Mössbauer data. In most cases, phase determinations are based on XRD data: Mössbauer is principally used to identify poorly crystalline or minor Fe-bearing phases. In Fe-bearing minerals with simple stoichiometry (e.g., magnetite), it is possible, with caution, to use Mössbauer to estimate a mode.

In the meteorites studied, absorptions were observed corresponding to ferrous Fe in olivine, pyroxene, and Fe-sulphides, Fe-Ni metal, a paramagnetic ferric phase (typically Fe-bearing clay or oxyhydroxides), and a magnetically ordered ferric phase (magnetite). Although the average stoichiometry of these phases within the meteorite are often not well-determined, precluding quantification from Mössbauer data alone, the recognition of the presence of a given phase is a useful guide in interpreting the XRD patterns. However, in the case of magnetite, we know the stoichiometry accurately (although, clearly, element substitution can complicate the analysis), and it is also easily recognized in Mössbauer spectra. ^{57}Fe Mössbauer spectra of magnetite typically show 2 sextets (6 line absorptions) at 298 K: one (at ~49 Tesla) arising from Fe^{3+} in tetrahedral "A" sites in the spinel structure, the other (at 45–46 Tesla) from mixed Fe^{2+}/Fe^{3+} in octahedral "B" sites. Because of electron hopping, the latter Fe^{2+}/Fe^{3+} gives an averaged subspectrum. "B" sites contain equal numbers of Fe^{2+} and Fe^{3+} ions, so ideally, we expect a 2:1 ratio in the spectral area of the 45 Tesla sextet to the 49 Tesla sextet. Although Mössbauer spectroscopy is not always a precise tool for mineral identification, no other common oxide or oxyhydroxide shows a sextet absorption at 45–46 Tesla at 298 K, with an association of a smaller sextet at 49 Tesla. Where estimates of modal abundance from Mössbauer data are made, they are only done for magnetite and are intended to provide a quantitative comparison with XRD phase quantification.

RESULTS AND DISCUSSION

Our XRD-PSD system detects all crystalline phases above ~0.5–1 wt%; Mössbauer analysis will detect Fe-bearing (including amorphous Fe-bearing phases) above 0.5 wt%. Amorphous Fe-poor materials are not detected, so some small component of the mineralogy will be excluded. Note also that where compositions are given for phases, these refer to the best fit standard.

Allende

Our Allende XRD-PSD pattern is shown in Fig. 3. Peak stripping using analyses of standard samples (shown here by constructing a simulated pattern from standards of different intensity) leaves a residual (also shown). As Allende is a
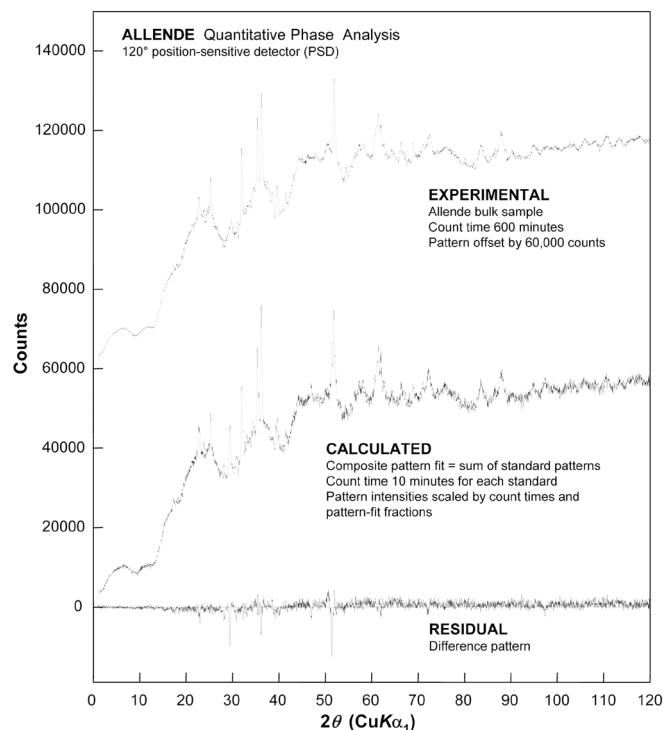
Fig. 3. Allende quantitative phase analysis by XRD-PSD. The diffraction pattern of the Allende bulk sample (count time of 600 min) is shown together with a composite pattern fit constructed by summing standard patterns. The intensity of each standard pattern (10 min count time) is multiplied by 60 then by a specific fraction to fit the Allende bulk pattern in the proportions: Fo$_{100}$ (7%), Fo$_{80}$ (11%), Fo$_{60}$ (23%), Fo$_{50}$ (27%), Fo$_{25}$ (7%), pentlandite (25%), plagioclase (0.5%), enstatite (3%), magnetite (0.7%), and Fe metal (0.8%). We then apply matrix absorption corrections (see Table 1) to estimate the phase proportions in the sample. Subtracting the composite standard pattern from the Allende pattern results in a near-zero residual, indicating that all the main phases have been identified. The fluorescent background of a crystalline pentlandite standard was used to model the X-ray amorphous sulphide in Allende; on subtraction, this results in the negative sharp peaks in the residual, but these do not affect the phase quantification in any way.

highly unequilibrated meteorite, the olivine peaks are broad and complex. We fit them based on analyses of standards over the range of the olivine solid solution and so obtain data relating to the abundance of different olivine compositions in our sample. Using the relevant mass absorption coefficients, we are able to convert the pattern intensities into a wt% for each phase, and with density data, into vol% (see Table 1). This analysis of Allende suggests (in wt%) Fo$_{100}$ (20.5%); Fo$_{80}$ (14.6%); Fo$_{60}$ (20.8%); Fo$_{50}$ (21.4%); Fo$_{25}$ (4.3%); enstatite (5.9%); plagioclase (0.9%); magnetite (0.3%); Fe-Ni metal (0.2%); and pentlandite (11.1%). For Fe-bearing phases, this is in line with our own and earlier Mössbauer analyses (see below). With the exception of mesostasis, other phases in Allende should be present at levels of <1 wt%.

In the case of Allende, where stoichiometry of constituent phases is rather well-known, it is possible to

Table 1. Abundance of individual phases within the Allende CV3 chondrite, determined byXRD-PSD. Phases identified (i) and their proportions (X_i) in the diffraction pattern relative to pure phase standards (proportion = 1.0) are shown together with attenuation values for Cu radiation, $(\mu/\rho)_i{}^{Cu}$, and for Fe radiation, $(\mu/\rho)_i{}^{Fe}$, used to make corrections for absorption in the calculation of final weight proportions. See the X-Ray Diffraction Methodology section for details.[a]

Phase i	XRD Pattern-fit fraction X_i	Mass absorption coefficient $(\mu/\rho)_i{}^{Cu}$	Mass absorption coefficient $(\mu/\rho)_i{}^{Fe}$	Density of phase i	Weight fraction Fe in phase i	Weight % of phase i	Volume % of phase i
Olivine (Fo$_{100}$)	0.07	32.2	63.0	3.22	0	20.5	23.4
Olivine (Fo$_{80}$)	0.11	71.3	63.0	3.46	.146	14.6	15.4
Olivine (Fo$_{60}$)	0.23	104.5	63.0	3.69	.269	20.8	20.6
Olivine (Fo$_{50}$)	0.27	119.2	62.9	3.81	.324	21.4	20.6
Olivine (Fo$_{25}$)	0.07	151.8	62.9	4.1	.446	4.3	3.9
Pentlandite	0.25[b]	146.7	95.0	5.08	.662	11.1	8.0
Clinoenstatite (En$_{90}$)	0.03	47.9	65.2	3.3	.054	5.9	6.6
Plagioclase (An$_{100}$)	0.005	52.7	100.5	2.76	0	0.9	1.2
Magnetite	0.007	223.3	57.1	5.2	.724	0.3	0.2
Fe-metal	0.008	304.4	70.4	7.88	1	0.2	0.1
Total	1.05[b]					100	100

[a]The calculated total wt% Fe is 24.7. The calculated grain density is 3.67 g cm^3.
[b]Fitted using background fluorescence signal only (X-ray amorphous phase), therefore, phase total need not necessarily be 1.0 before correction for fluorescence (see XRD Methodology in the text).

convert our modal data into an estimate of bulk chemistry, which we can then compare with literature data (Jarosewich 1990) as a check on our modal assessment. Comparing elements with abundance >1 wt% (Si, Fe, Mg, O, Al, Ca, S), we find an average deviation, between modal "chemical" data and literature chemical data for a given element, of 1.2 wt% (illustrated graphically in Fig. 4), evidence that our XRD data are approximating a modal mineralogy for Allende.

Deriving a complete modal mineralogy for a sample is also an effective method of estimating its grain density, since the densities of individual mineral species are well-known. This is an attractive alternative to helium pycnometry, since it is also applicable to extremely small samples and is non-invasive. As Consolmagno and Britt (1998) have outlined a simple method for determining bulk density in meteorites, the combination of techniques should allow bulk density and grain density (and, therefore, porosity) to be determined routinely. In the case of Allende, the measured assemblage suggests a grain density of 3.67 g cm^{-3} (close to the measured value of 3.53 g cm^{-3} [Britt and Consolmagno 2003]).

As discussed above, Cu$K\alpha_1$ radiation gives rise to a large fluorescent background when a sample contains abundant Fe. The Allende background indicates 24.7 wt% Fe, very close to the published value of 23.8 wt% (Kallemeyn and Wasson 1981; Jarosewich 1990). As each Fe-bearing phase contributes to the background, we can use the background intensity to infer the presence of a mineral with the Fe content of a sulphide (see above in the X-ray Diffraction Methodology section). Although there are few well-defined peaks for pentlandite (the bulk of it may be present as very fine grained matrix phase), Mössbauer studies have detected it (e.g., Hoffman et al. 2001).

Mössbauer spectroscopy studies of Allende (Roy-Poulson et al. 1981; Oliver et al. 1983; Fisher and Burns
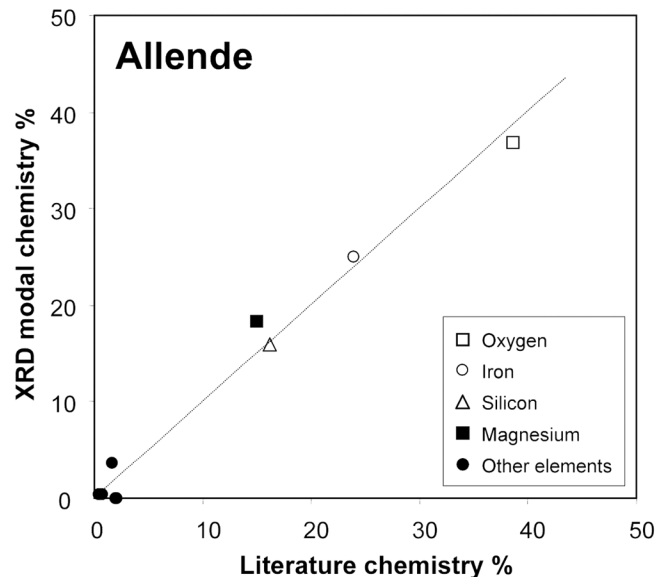
Fig. 4. A comparison of single element data obtained from the literature for Allende (Jarosewich 1990) and calculated from our XRD-derived mineralogical data. There is a 1:1 correlation between the 2 data sets with R^2 of 0.99, indicating that the bulk chemistry compositions derived from the XRD mineralogy are almost identical to the literature values and suggesting that we can be reasonably confident in our modal assessment. The small divergence for Mg is most likely a result of our limited set of olivine standards being a less than perfect match to the complete range of olivine compositions present in Allende.

1991; Bland et al. 1995; Hoffman et al. 1999, 2000, 2001) have observed components in spectra associated primarily with olivine (75–80% of the total Fe), minor pentlandite (occasionally confused with a paramagnetic Fe^{3+} phase) making up ~15% of total Fe, and minor troilite (2%) or chromite. Hoffman et al. (2000) found a minor magnetic

ferric phase associated with magnetite, but this appears atypical (none was observed by previous workers). The absence of magnetite in other spectra suggests an upper limit of 0.5 wt% on its abundance in Allende (Bland et al. 1999). A saturation magnetization study also failed to detect magnetite, putting an upper limit of 1 wt% on its abundance (Hyman and Rowe 1986). Although magnetite has been recognized in Allende petrographically, the fact that a large number of studies, using a range of instrumental techniques on a variety of Allende bulk samples, have failed to detect it suggests that it is present at a rather low level of abundance in this meteorite (<0.5 wt%, or <0.3 vol%). Sample heterogeneity is unlikely to be the cause, as each study used different aliquots of the meteorite. This appears to be something of a departure from the general perception that Allende has experienced substantial oxidation and is relatively abundant in magnetite. Petrographic studies of Allende commonly observe magnetite in situ (e.g., Krot et al. 1998); however, estimating modal abundance in the whole rock is extremely difficult using these techniques. The only other quantitative estimate of magnetite abundance in Allende was an optical point counting study which estimated 1.2 vol% (McSween 1977). If magnetite were as abundant as 1.2 vol% in Allende, it would be easily detected by Mössbauer, XRD, and saturation magnetization. Possibly, the point counting study may have included more than 1 minor opaque phase in its magnetite determination. In contrast to Allende, Vigarano has been shown to contain a significant proportion of magnetite, at around the 4.3 wt% (2.5 vol%) level (Bland et al. 1997, 1999). Although other data have clearly shown that the distinction between oxidized and reduced CVs has genetic significance, it does not appear to be related to the abundance of magnetite, as was previously thought.

Murchison

CM meteorites contain abundant matrix, much of which is a poorly characterized phase that has been shown to be composed largely of tochilinite and cronstedtite, along with minor amounts of other phases such as magnetite and chromite (e.g., Tomeoka and Buseck 1985; Nakamura and Nakamuta 1996). Serpentine is the other major constituent of CM matrix (Zolensky et al. 1993). Olivine and pyroxene are observed in chondrules, but small crystals and clasts of these minerals are also found in matrix (Barber 1981). Small amounts of Fe-Ni metal, pyrrhotite, pentlandite, saponite, phosphates, clinochlore, carbonates, and variable magnetite are also observed (Mackinnon 1980; Barber 1981; Zolensky and McSween 1988; Scott et al. 1988; Zolensky et al. 1993).

XRD-PSD analysis of Murchison suggests Fo_{100} (7.4%); Fo_{80} (2.2%); Fo_{50} (2%); enstatite (2.2%); pyrrhotite (2.9%); pentlandite (0.5%); magnetite (0.4%); serpentine (22.8%); calcite (1.1%); and cronstedtite/tochilinite (58.5%), which includes the interstratified 17.8 Å phase. These estimates are compatible with the Mössbauer results. Based on this assemblage, we calculate a grain density of 2.93 g cm^{-3}. Earlier measurements of grain density in Murchison (Britt and Consolmagno 2003) varied around 2.86 ± 0.03 g cm^{-3}, quite close to our estimate.

Earlier Mössbauer studies (Morris et al. 1994) and our own analysis of Murchison show absorptions corresponding to ferrous Fe in olivine, pyroxene, and a paramagnetic ferric phase (probably Fe-bearing phyllosilicate).

Tagish Lake

Tagish Lake is a breccia consisting of 2 major lithologies, carbonate-poor and carbonate-rich, with carbonate-poor being slightly more abundant (Zolensky et al. 2002). Sparse, heavily aqueously altered chondrules are found with a few remnant olivine grains intact (Fo_{99} mode), and sparse CAIs and aggregates containing olivine ± pyroxene are also observed (Zolensky et al. 2002). In addition, a variety of loose grains of olivine, magnetite, Fe-Ni sulphide, Cr-Ni phosphide, and carbonates are found in a matrix that consists mainly of saponite, serpentine, and Fe-Ni sulphides (mostly pyrrhotite) (Zolensky et al. 2002). The carbonate-rich lithology is similar, although saponite is by far the most common phyllosilicate. Magnetite is rare, and Fe-Mg-Ca-Mn carbonates are very abundant (Zolensky et al. 2002).

Our XRD-PSD study of Tagish Lake suggests Fo_{100} (7.9%); Fe-bearing carbonate (14.4%); pyrrhotite (8.5%); pentlandite (0.6%); magnetite (8.3%); and interstratified saponite-serpentine clay (60.3%). Other phases are, of course, present but probably at levels of <1 wt%. The high magnetite abundance that we measure suggests our sample may be from the carbonate-poor Tagish Lake lithology (Mössbauer analyses of sub-samples of this material showed little variation in magnetite abundance suggesting that any contamination with the carbonate-rich lithology was minimal).

Based on this data, we calculate a grain density of 2.84 g cm^{-3} for Tagish Lake. Although a bulk density measurement of 1.67 g cm^{-3} has been made for this meteorite (Zolensky et al. 2002), no measurement of porosity or grain density on the Tagish Lake meteorite has been performed. With our grain density estimate, and the measured bulk density, we can, therefore, calculate a porosity for Tagish Lake. Our data suggest that this meteorite has an extremely high porosity of 41%, similar to some chondritic IDPs (e.g., Corrigan et al. 1997) but much higher than any value measured for a bulk meteorite. This porosity is extremely close to an estimate of ~40% that was based on an entry model for the Tagish Lake fireball (Brown et al. 2002).

Tagish Lake has not been previously analyzed by Mössbauer spectroscopy (see spectrum in Fig. 5). The Mössbauer analysis, which suggests 8.5 wt% magnetite, is very close to our XRD estimate. Despite the correspondence

Table 2. Abundance of individual phases within the Murchison CM2 chondrite, determined by XRD-PSD. See Table 1 and the text for details of how final weight proportions are derived. For serpentine, we assume an Mg-rich serpentine: $Mg_{2.9}Fe_{0.1}Si_2O_5(OH)_4$. The enstatite composition is from Fuchs et al (1973).[a]

Phase i	XRD Pattern-fit fraction X_i	Mass absorption coefficient $(\mu/\rho)_i^{Cu}$	Mass absorption coefficient $(\mu/\rho)_i^{Fe}$	Density of phase i	Weight fraction Fe in phase i	Weight % of phase i	Volume % of phase i
Olivine (Fo_{100})	0.03	32.2	63.0	3.22	0	7.4	6.8
Olivine (Fo_{80})	0.02	71.3	63.0	3.46	.146	2.2	1.9
Olivine (Fo_{50})	0.03	119.2	62.9	3.81	.324	2.0	1.6
Clinoenstatite (En_{98})	0.01	36.4	65.3	3.3	.011	2.2	1.9
Pyrrhotite	0.05	138.1	98.1	4.58	.604	2.9	1.8
Pentlandite	0.01	146.7	95.0	5.08	.662	0.5	0.3
Magnetite	0.01	223.3	57.1	5.2	.724	0.4	0.2
Serpentine	0.10	35.1	58.4	2.55	.02	22.8	26.2
Cronstedtite	0.73[b]	103.5	58.4	2.95	.272	58.5	58.1
Calcite	0.01	74.4	139.4	2.72	0	1.1	1.2
Total	1.00					100	100

[a]The calculated total wt% Fe is 19.7. The calculated grain density is 2.93 g cm^3.
[b]Fitted using background fluorescence signal only (poorly crystalline phase). The weight fraction Fe in cronstedtite was calculated from Browning et al. (1996) for average matrix "serpentine" (which is typically a cronstedtite-serpentine mixture).

Table 3. Abundance of individual phases within the Tagish Lake anomalous C2 chondrite, determined by XRD-PSD. See Table 1 and the text for details of how final weight proportions are derived. Compositions of phyllosilicate and carbonate are from Gounelle et al (2001) and Zolensky et al. (2002).[a]

Phase i	XRD Pattern-fit fraction X_i	Mass absorption coefficient $(\mu/\rho)_i^{Cu}$	Mass absorption coefficient $(\mu/\rho)_i^{Fe}$	Density of phase i	Weight fraction Fe in phase i	Weight % of phase i	Volume % of phase i
Olivine (Fo_{100})	0.03	32.2	63.0	3.22	0	7.9	7.0
Fe-Mg carbonate	0.18	105.0	48.3	3.5	.299	14.4	11.7
Pyrrhotite	0.14	138.1	98.1	4.58	.604	8.5	5.3
Pentlandite	0.01	146.7	95.0	5.08	.662	0.6	0.3
Magnetite	0.22	223.3	57.1	5.2	.724	8.3	4.5
Saponite-serpentine	0.42	58.7	64.9	2.4	.094	60.3	71.2
Total	1.00					100	100

[a]The calculated total wt% Fe is 21.5. The calculated grain density is 2.84 g cm^3, and porosity is 41%.

between the Mössbauer results and XRD, we explored the possibility that there might be a nanophase Fe-bearing component in Tagish Lake, as is observed in Orgueil. However, low temperature Mössbauer spectroscopy suggests that any superparamagnetic component (whether magnetite or ferrihydrite) is minor in this meteorite (Bland et al. 2002). In contrast, Orgueil contains significant ferrihydrite (Tomeoka and Buseck 1988) in a superparamagnetic form (Wdowiak and Agresti 1984; Madsen et al. 1986).

Orgueil

Tomeoka and Buseck (1988) performed a detailed petrographic and TEM study of Orgueil and reviewed the existing literature. They found that Orgueil matrix consists of Fe-bearing, Mg-rich serpentine and smectite (saponite), as well as a poorly crystalline Fe-rich material containing minor S and Ni—probably ferrihydrite. Magnetite is abundant, as are veins of Mg-, Ca-sulphate (possibly produced after the meteorite fell [Gounelle and Zolensky 2001]). Our XRD analysis of Orgueil indicates Fo_{100} (2.4%); Fo_{80} (3.3%), Fo_{60}

(1.5%); troilite (2.1%); pyrrhotite (4.4%); magnetite (9.7%); serpentine (7.3%); saponite-serpentine (64.2%); and ferrihydrite (5.0%). This assemblage suggests a grain density of 2.76 g cm^{-3} (the published value is 2.43 g cm^{-3} [Consolmagno and Britt 1998], although Gounelle and Zolensky [2001] note that bulk measurements of CI chondrites are highly variable).

The magnetite and ferrihydrite estimates are consistent with earlier work (Hyman and Rowe 1986; Tomeoka and Buseck 1988; Wdowiak and Agresti 1984) and our own Mössbauer analysis, which suggests 10.6 wt% magnetite. A surprising result (confirmed by Mössbauer) is the detection of appreciable fayalitic olivine.

To investigate modal heterogeneity in Orgueil mineralogy, and any association, linked to localized variations in the degree of aqueous alteration in the meteorite, between anhydrous and hydrous species, 10 different aliquots of Orgueil were analyzed in a micro-well with a volume of 0.07 mm^3 using the MicroSource®. The averaged bulk mineralogical data are the same as obtained for the macro-well using a conventional source. However, by analyzing small

Table 4. Abundance of individual phases within the Orgueil CI1 chondrite determined by XRD-PSD. See Table 1 and the text for details of how final weight proportions are derived. The composition of Fe-bearing, Mg-rich serpentine is taken from Tomeoka and Buseck (1988). The composition of the saponite-serpentine (approximately equal proportions) disordered interstratified phase is taken from Tomeoka and Buseck (1988).[a]

Phase i	XRD Pattern-fit fraction X_i	Mass absorption coefficient $(\mu/\rho)_i^{Cu}$	Mass absorption coefficient $(\mu/\rho)_i^{Fe}$	Density of phase i	Weight fraction Fe in phase i	Weight % of phase i	Volume % of phase i
Olivine (Fo_{100})	0.01	32.2	63.0	3.22	0	2.4	2.1
Olivine (Fo_{80})	0.03	71.3	63.0	3.46	.146	3.3	2.6
Olivine (Fo_{60})	0.02	104.5	63.0	3.69	.269	1.5	1.1
Troilite	0.04	146.0	107.9	4.7	.635	2.1	1.2
Pyrrhotite	0.08	138.1	98.1	4.58	.604	4.5	2.7
Magnetite	0.28	223.3	57.1	5.2	.724	9.7	5.1
Serpentine	0.05	53.0	58.4	2.6	.086	7.3	7.7
Saponite-serpentine	0.40	48.1	57.3	2.4	.070	64.2	73.8
Ferrihydrite	0.10[b]	181.4	49.8	3.8	.581	5.0	3.7
Total	1.01[b]					100	100

[a]The calculated total wt% Fe is 20.0. The calculated grain density is 2.76 g cm[3].

[b]Fitted using background fluorescence signal only (X-ray amorphous phase), therefore, phase total need not necessarily be 1.0 before correction for fluorescence. Based on background fluorescence appears to be almost identical to amorphous Fe_2O_3.
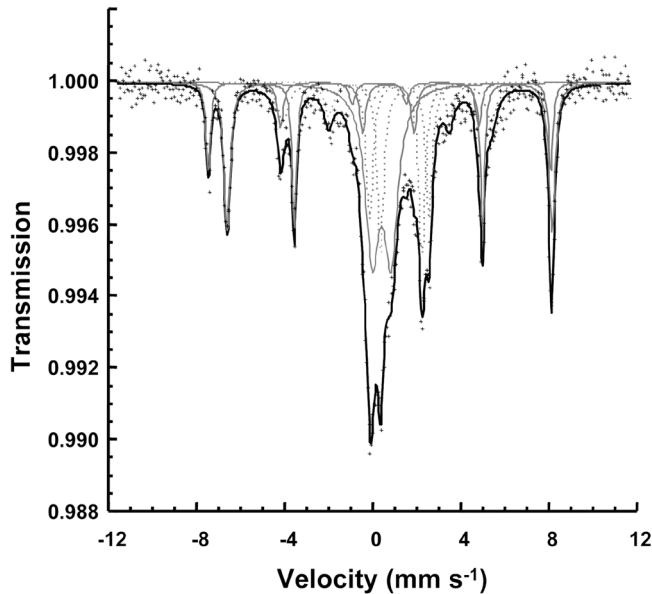
Fig. 5. [57]Fe Mössbauer spectrum of Tagish Lake. Two sets of 6-line absorptions (sextets) associated with magnetite are especially prominent, as are doublets probably associated with Fe-bearing phyllosilicate and carbonate.

Fig. 6. Modal abundance data for small (0.07 mm[3]) aliquots of Orgueil, derived from MicroSource® XRD analysis, shown as stacked columns. 10 samples were analyzed. Here, we show data collected from 5 representative aliquots, ranked in order of decreasing olivine abundance. Orgueil is dominated by saponite-serpentine. The data show significant variation in Orgueil modal mineralogy at a fine scale and indicate that olivine varies inversely with saponite-serpentine.

volumes of material, it is possible to observe mineralogical heterogeneity within Orgueil. We find that the proportions of all mineral phases, apart from pyrrhotite, vary between 5 and 20 wt%, which is well beyond the expected range of error on the data. Pyrrhotite abundances vary on the order of 2 wt%. Figure 6 shows data from 5 representative samples.

We observe an inverse correlation between the proportions of olivine and saponite-serpentine, with olivine diminishing in abundance as saponite-serpentine increases (see Fig. 6). Given that there is no major change in the proportion of sulphide, it appears likely that the relationship observed between olivine and saponite-serpentine is genuine and that saponite-serpentine has formed by aqueous alteration of olivine. No evidence exists to suggest that Orgueil has undergone metamorphism, which would have dehydrated original phyllosilicate material to form olivine, as so the olivine now present in Orgueil is likely to be a remnant phase. This is consistent with the oxygen isotopic analyses of olivine and pyroxene carried out by Leshin et al. (1997), who suggest that anhydrous phases in Orgueil are primary minerals—the remains of chondrule phenocrysts. It is clear that aqueous alteration did not go to completion in Orgueil and that the intensity of alteration varies significantly at a fine scale; and it appears likely that Orgueil was initially composed primarily of anhydrous materials.

Limitations of the Technique

The primary limitation of the combined XRD-PSD/ Mössbauer spectroscopy method is the need for an extensive database of mineral standards to deconvolve complex X-ray patterns. This is apparent in the data for olivine in Allende: there is a solid solution in olivine compositions, but at present, we are limited to a relatively small number of monomineralic olivine standards. Similarly, it is often necessary to compromise and use standards with similar compositions and structures when unusual sulphides or phyllosilicates are not available. In the worst case, this could lead to the misidentification of a phase with possibly similar composition and structure. As our database of standards improves, we will be able to refine our phase identification and quantification.

As noted earlier, we cannot detect or quantify amorphous Fe-poor materials using this method. However, their presence could be inferred if we noted a sharp divergence between the bulk chemistry estimated from our modal assessment and literature data. We observe no such divergence. The abundance of poorly crystalline Fe-bearing phases may be estimated from Mössbauer data and by making use of Fe-fluorescence in the XRD patterns, although, in this case, phase quantification will be less accurate than for crystalline materials. Low temperature Mössbauer studies of specific meteorites containing abundant amorphous phases will reduce this problem.

At present, minerals with abundances of <0.5–1 wt% will not be detected by either technique. However, the recent upgrade of our XRD-PSD system with a high-brightness X-ray MicroSource® now allows identification and quantification of the mineralogy of selected areas within meteorites at high spatial resolution, improving the quantification of trace mineralogy.

CONCLUSIONS

We have outlined several advances in X-ray diffraction that are of relevance to the analysis of primitive meteorites. Although this is a preliminary study, we have several reasons to be confident that our XRD modal mineralogy assessments are approximating actual mineral abundance. As $CuK\alpha_1$ radiation gives rise to a fluorescent background proportional to the abundance of Fe, we arrive at an independent estimate of bulk Fe wt% in the sample, which compares favorably with literature data. In addition, where the stoichiometry of constituent phases is well-known, as in the case of Allende, converting our modal data into an estimate of bulk chemistry is possible, which we can then compare with literature data. This provides an additional check on our abundance estimates. The comparison of XRD and Mössbauer spectroscopy data for magnetite is also favorable. The correspondence between these different techniques (one based on long-range order within materials and the other on

short-range order) suggests that we also have reason to be confident in the non-Fe-bearing estimates. Finally, in cases where published grain density measurements exist, we are able to compare these data to our calculated values, providing an additional independent test of our modal abundance estimate for each meteorite. Our grain density estimates are close to literature values, typically ~0.2 g cm^{-3} above the published grain density. This overestimate may be real, since helium pyconometry analysis will not detect unconnected porosity. The implication is that meteorite porosity may be slightly higher than previously supposed. Overall, comparing our XRD modal estimates with a variety of other data (literature chemistry, previously published abundances of some phases, Mössbauer data, and published grain densities) suggests that our phase quantification estimates are close to the actual mineral abundances within each meteorite.

As well as quantifying the abundance of individual minerals, where silicates are unequilibrated (given appropriate standards), we can place constraints on the abundance of individual compositions within a solid solution, as illustrated in the case of Allende where fayalitic olivine makes up a significant proportion of the total mineral compliment. Given that the origin of fayalitic olivine remains a topic of discussion, applying this approach to other CV chondrites to discern whether the abundance of a given olivine composition correlates with any other chondrite properties will be particularly interesting.

Comparing how mineralogy varies on a small scale in a meteorite is also useful. The analysis of different aliquots of Orgueil using MicroSource® XRD-PSD suggests not only that aqueous alteration was an incomplete process in the CIs but that the degree of alteration varies substantially on a small scale and that the abundance of olivine varies inversely with phyllosilicates. The suggestion is that Orgueil was initially primarily composed of anhydrous materials before it experienced aqueous alteration that was variable on the mm-scale. This analysis illustrates the potential of the MicroSource® XRD-PSD. A similar analytical approach could be taken to quantify the mineralogy in chondrite inclusions, as well as a variety of other extraterrestrial materials. When combined with other analyses (trace element data, oxygen isotopes, etc.), MicroSource® XRD-PSD promises to be a useful tool in understanding the formation and evolution of extraterrestrial materials.

Finally, the ability to not only calculate modal mineralogy but to use that data to determine a grain density for a meteorite is a significant advance. As bulk density can be easily measured (Consolmagno and Britt 1998), the physical properties of a meteorite can be determined routinely. The grain density we determine for Tagish Lake based on its modal mineralogy, combined with a literature bulk density value, suggests that, at 41%, this sample has the highest porosity yet measured in a meteorite.

With the exception of amorphous, Fe-poor phases and

phases below 0.5–1 wt% abundance, the combined XRD-PSD/Mössbauer methodology appears capable of quantifying the complete modal mineralogy of even highly unequilibrated chondrites containing abundant fine-grained matrix. This data may be of value in interpreting various aspects of chondrite chemistry and isotopic composition, as well as IR spectra of carbonaceous asteroids. The advent of MicroSource® XRD allows us to perform modal abundance analysis on volumes of material as small as 0.02 mm³, opening up a wide range of analytical targets. Since unequilibrated chondrites constitute the most formidable analytical challenge for our technique, we anticipate that a large variety of other extraterrestrial materials should be amenable to this type of analysis.

*Editorial Handling—*Dr. David Mittlefehldt

REFERENCES

Barber D. J. 1981. Matrix phyllosilicates and associated minerals in C2M carbonaceous chondrites. *Geochimica et Cosmochimica Acta* 45:945–970.

Batchelder M. and Cressey G. 1998. Rapid, accurate phase quantification of clay-bearing samples using a position-sensitive X-ray detector. *Clays and Clay Minerals* 46:183–194.

Bland P. A. and Cressey C. 2001. Modal mineralogy of unequilibrated meteorites by X-ray diffraction and Mössbauer spectroscopy (abstract #1853). 32nd Lunar and Planetary Science Conference. CD-ROM.

Bland P. A., Berry F. J., and Pillinger C. T. 1995. Weathering effects in the Axtell CV3 carbonaceous chondrite. 26th Lunar and Planetary Science Conference. pp. 133–134.

Bland P. A., Sephton M. A., Bevan A. W. R., Berry F. J., Cadogan J. M., and Pillinger C. T. 1997. *Magnetite in Vigarano: An iron-57 Mössbauer spectroscopy study.* Houston: Lunar and Planetary Institute. LPI Technical Report 97–02. p. 3.

Bland P. A., Hoffman E., Jones R., Cressey G., and Cadogan J. M. 1999. Magnetite in "oxidized" and "reduced" CV chondrites (abstract). *Meteoritics & Planetary Science* 34:A12–A13.

Bland P. A., Hoffman E., Krot A. N., and Berry F. J. 2000a. CV3 chondrites: How oxidized or reduced? *Meteoritics & Planetary Science* (abstract) 35:A28.

Bland P. A., Cressey G., and Russell S. S. 2000b. Toward a laboratory-based X-ray microprobe for the characterization and quantification of phases in meteorites (abstract). *Meteoritics & Planetary Science* 35:A27–A28.

Bland P. A., Cressey G., Alard O., Rogers N. W., Forder S. D., and Gounelle M. 2002. Modal mineralogy of carbonaceous chondrites and chemical variation in chondrite matrix (abstract #1754). 33rd Lunar and Planetary Science Conference.

Britt D. T. and Consolmagno G. J. 2003. Stony meteorite porosities and densities: A review of the data through 2001. *Meteoritics and Planetary Science* 38:1161–1180.

Brown P. G., ReVelle D. O., Tagliaferri E., and Hildebrand A. R. 2002. An entry model for the Tagish Lake fireball using seismic, satellite, and infrasound records. *Meteoritics & Planetary Science* 37:661–675.

Browning L. B., McSween H. Y., Jr., and Zolensky M. E. 1996. Correlated alteration effects in CM carbonaceous chondrites. *Geochimica et Cosmochimica Acta* 60:2621–2633.

Consolmagno G. J. and Britt D. T. 1998. The density and porosity of meteorites from the Vatican collection. *Meteoritics & Planetary Science* 33:1231–1241.

Corrigan C. M., Zolensky M. E., Dahl J., Long M., Weir J., and Sapp C. 1997. The porosity and permeability of chondritic meteorites and interplanetary dust particles. *Meteoritics & Planetary Science* 32:509–515.

Cressey G. and Batchelder M. 1998. Dealing with absorption and microabsorption in quantitative phase analysis. *International Union of Crystallography Newsletter* 20:16–17.

Cressey G. and Schofield P. F. 1996. Rapid whole-pattern profile-stripping method for the quantification of multiphase samples. *Powder Diffraction* 11:35–39.

Fisher D. S. and Burns R. G. 1991. Pre-terrestrial oxidation products of iron minerals in carbonaceous meteorites identified in Mössbauer spectra. 22nd Lunar and Planetary Science Conference. pp. 389–390.

Fuchs L. H., Olsen E., and Jensen K. J. 1973. Mineralogy, crystal chemistry, and composition of the Murchison (C2) meteorite. *Smithsonian Contributions to the Earth Sciences* 10:1–39.

Gounelle M. and Zolensky M. E. 2001. A terrestrial origin for sulfate veins in CI1 carbonaceous chondrites. *Meteoritics & Planetary Science* 36:1321–1329.

Gounelle M., Zolensky M. E., Tonui E., and Mikouchi T. 2001. Mineralogy of Tagish Lake, a unique type 2 carbonaceous chondrite (abstract #1616). 32nd Lunar and Planetary Science Conference. CD-ROM.

Hoffman E., Seifu D., and Oliver F. W. 1999. Axtell and Allende: A Mössbauer spectroscopic comparison (abstract #1950). 30th Lunar and Planetary Science Conference. CD-ROM.

Hoffman E., Seifu D., and Oliver F. W. 2000. Axtell and Allende: A Mössbauer spectroscopic study. *Meteoritics & Planetary Science* 35:431–434.

Hoffman E., Housley R. M., Bland P. A., Seifu D., and Oliver F. W. 2001. Fe-rich pentlandite in Allende bulk samples and separates: A Mössbauer spectroscopic analysis (abstract #2116). 32nd Lunar and Planetary Science Conference. CD-ROM.

Hyman M. and Rowe M. W. 1986. Saturation magnetization measurements of carbonaceous chondrites. *Meteoritics* 21:1–22.

Jarosewich J. 1990. Chemical analyses of meteorites: A compilation of stony and iron meteorite analyses. *Meteoritics* 25:323–337

Kallemeyn G. W. and Wasson J. T. 1981. The compositional classification of chondrites: I. The carbonaceous chondrite groups. *Geochimica et Cosmochimica Acta* 45:1217–1230.

Krot A. N., Petaev M. I., Scott E. R. D., Choi B K., Zolensky M. E., and Keil K. 1998. Progressive alteration in CV3 chondrites: More evidence for asteroidal alteration. *Meteoritics & Planetary Science* 33:1065–1085.

Leshin L. A., Rubin A. E., and McKeegan K. D. 1997. The oxygen isotopic composition of olivine and pyroxene from CI chondrites. *Geochimica et Cosmochimica Acta* 61:835–845.

Madsen I. C. 1999. Quantitative phase analysis round robin. *International Union of Crystallography Newsletter* 22:3–5.

Madsen I. C., Scarlett N. V. Y., Cranswick L. M. D., and Lwin T. 2001. Outcomes of the International Union of Crystallography Commission on Powder Diffraction round robin on quantitative phase analysis: Samples 1a to 1h. *Journal of Applied Crystallography* 34:409–426.

Madsen M. B., Morup S., Costa T. V. V., Knudsen J. M., and Olsen M. 1986. Superparamagnetic component in the Orgueil meteorite and Mössbauer spectroscopy studies in applied magnetic fields. *Nature* 321:501–503.

MacKinnon I. D. R. 1980. Structures and textures of the Murchison

and Mighei carbonaceous chondrite matrices. Proceedings, 11th Lunar and Planetary Science Conference. pp. 839–853.

McSween H. Y., Jr., Bennett M. E., and Jarosewich E. 1991. The mineralogy of ordinary chondrites and implications for asteroid spectrophotometry. *Icarus* 90:107–116.

McSween H. Y., Jr. 1977. Petrographic variations among carbonaceous chondrites of the Vigarano type. *Geochimica et Cosmochimica Acta* 41:1777–1790.

Menzies O. N., Bland P. A., and Berry F. J. 2001. An [57]Fe Mössbauer study of the metamorphic sequence in unequilibrated ordinary chondrites (abstract). *Meteoritics & Planetary Science* 36:A131.

Menzies O. N., Bland P. A., Cressey G., and Berry F. J. 2002. A quantitative modal mineralogy study of ordinary chondrites using X-ray diffraction and Mössbauer spectroscopy (abstract #1500). 33rd Lunar and Planetary Science Conference. CD-ROM.

Mullane E., Russell S. S., Gounelle M., and Mason T. F. D. 2003. Iron isotope composition of Allende and Chainpur chondrules (abstract #1027). 34th Lunar and Planetary Science Conference. CD-ROM.

Morris R. V., Zolensky M. E., Hiroi T., and Lipschutz M. E. 1994. Mössbauer mineralogy of calcined Murchison meteorite. 25th Lunar and Planetary Science Conference. pp. 941–942.

Nakamura T. and Nakamuta Y. 1996. X-ray study of PCP from the Murchison CM carbonaceous chondrite. *Proceedings of the NIPR Symposium on Antarctic Meteorites* 9:37–50.

Oliver F. W., Isuk E. E., and Wynter C. 1984. Mössbauer study of the Allende meteorite. *Meteoritics* 19:25–27.

Roy-Poulson H., Larsen L., Roy-Poulson N. O., and Vistisen L. 1981. Meteorites and the origin of water and reduced carbon on the Earth. *Physica Scripta* 23:1113–1117.

Scott E. R. D., Barber D. J., Alexander C. M., Hutchison R., and Peck J. A. 1988. Primitive material surviving in chondrites: Matrix. In *Meteorites and the early solar system,* edited by Kerridge J. F. and Matthews M. S. Tucson: University of Arizona Press. pp. 718–715.

Tomeoka K. and Buseck P. R. 1985. Indicators of aqueous alteration in CM carbonaceous chondrites: Microtextures of a layered mineral containing Fe, S, O, and Ni. *Geochimica et Cosmochimica Acta* 49:2149–2163.

Tomeoka K. and Buseck P. R. 1988. Matrix mineralogy of the Orgueil CI carbonaceous chondrite. *Geochimica et Cosmochimica Acta* 52:1627–1640.

Wdowiak T. J. and Agresti D. G. 1984. Presence of a superparamagnetic component in the Orgueil meteorite. *Nature* 311:140–142.

Zhu X. K., Guo Y., O'Nions R. K., Young E. D., and Ash R. D. 2001. Isotopic homogeneity of iron in the early solar nebula. *Nature* 412:311–313.

Zolensky M. and McSween H. Y., Jr. 1988. Aqueous alteration. In *Meteorites and the early solar system,* edited by Kerridge J. F. and Matthews M. S. Tucson: University of Arizona Press. pp. 114–143.

Zolensky M., Barrett R., and Browning L. 1993. Mineralogy and composition of matrix and chondrule rims in carbonaceous chondrites. *Geochimica et Cosmochimica Acta* 57:3123–3148.

Zolensky M. E, Nakamura K., Gounelle M., Mikouchi T., Kasama T., Tachikawa O., and Tonui E. 2002. Mineralogy of Tagish Lake: An ungrouped type 2 carbonaceous chondrite. *Meteoritics & Planetary Science* 37:737–761.